AFWAL-TR-81-4019
Volume II

ACCELERATED TESTING IN CONTROLLED ATMOSPHERES

M. Khobaib and Frank C. Chang*
Systems Research Laboratories, Inc.
2800 Indian Ripple Road
Dayton, OH 45440

C. T. Lynch
Air Force Wright Aeronautical Laboratories
AFWAL/MLLN
Wright-Patterson Air Force Base
OH 45433

*Present address: Army Materials and Mechanics Research Center, Watertown, MA 02172

ABSTRACT

Available methods for accelerated testing of corrosion behavior do not yield accurate or reliable results for predicting the service life of aircraft components and materials which degrade or fail due to environmental attack. Research has been conducted in controlled atmospheres on the localized environmental enhancement of crack-growth rates of aerospace alloys in order to provide the basis for development of realistic accelerated corrosion tests. Initial emphasis has been placed on investigations of environmental conditions for accelerating reactions which lead to catastrophic failure of high-strength alloys. Corrosion-fatigue and rising-load experiments have been conducted on 4340 steel and 7075-T6 aluminum using accelerating pollutants such as sulfur dioxide and ambient air to 100% relative humidity (RH) air in a specially designed atmospheric chamber. Initial results indicate that a realistic environmental enhancement of crack-growth rates can be employed to develop accelerated tests which can be related to actual in-service degradation. For materials with high stress-corrosion susceptibility, the threshold for crack growth (K_{ISCC}) was estimated to be 45 - 46 MPa $\sqrt{m}$ for 4340 steel at a 1440-MPa yield-strength level, as compared to 49 - 52 MPa $\sqrt{m}$ as determined by means of rising-load tests and 44 - 46 MPa $\sqrt{m}$ by fracture analysis in 1000 ppm SO_2 at 80% RH. Thus, a rapid and reproducible method for K_{ISCC} determination appears feasible.

INTRODUCTION

The enormous cost of corrosion prevention and control for aircraft has been brought to light in a recent report published by NBS [1]. Several similar studies have been conducted within the Air Force regarding the total cost of corrosion prevention and control for aircraft. The inescapable conclusion is that total corrosion costs in terms of life-cycle management and maintenance of aircraft represent an intolerable burden to the Air Force in maintaining force effectiveness at a reasonable cost to the taxpayer. The 1978 NBS report [1] estimated the total corrosion cost to be 70 billion dollars nationally. For the Air Force the direct cost of corrosion maintenance in the field and at the depot level was estimated at that time to be 750 million dollars, and the total corrosion cost including facilities was estimated to be in excess of one billion dollars. During the 1975 and 1977 AFOSR-AFML Corrosion Workshops, improved accelerated tests were cited as being a major area of need requiring further research [2,3]. One of the major problems in effectively reducing aircraft-corrosion maintenance costs has been the inability of the research community to develop realistic corrosion tests which give meaningful results in a reasonable length of time. Despite the need for this development, there are no accurate methods for accelerated testing for corrosion which yield reliable results for predicting the service life of aircraft components and materials which degrade or fail due to environmental attack. Current alternatives involve the use of 1) gross tests such as salt-water immersion which yield relative corrosivity values that have no quantitative relation to service life or 2) outdoor atmospheric exposure tests which require experiments of three to five years duration or longer and are specific to one local environment. Furthermore, the immersion tests make use of high salt concentrations which do not represent realistic conditions, except for marine environments. Thus, the results have no real-time basis for extrapolation to real conditions. Fundamentally, the corrosion reactions from immersion tests are completely different from those in typical high-humidity air environments containing small concentrations (ppm to ppb range) of contaminants (e.g., SO_2, NO_X, Cl^-) which accelerate the corrosion reactions.

Therefore, we have initiated a program to provide the basis for the development of realistic accelerated tests which can be used to predict the long-range corrosion behavior of materials under actual service conditions. Test environments are based upon reasonable variations in the concentration of corrosion-accelerating pollutants, humidity, and temperature, using primary and secondary air-quality standards to establish concentration base levels for accelerating pollutants such as sulfur dioxide. Controlled atmospheric experiments are being conducted for general corrosion and for localized environmental enhancement of crack-growth rates. Crack-growth studies include low-cycle corrosion-fatigue, rising-load, and constant-slow-strain-rate tests. Some of the results are reported in this paper for 4340 steel and 7075-T6 aluminum alloys under rising load and low-cycle fatigue.

The state-of-the-art in accelerated-corrosion testing methods as described in the ASTM Book of Standards and approved by NACE requires the aforementioned use of gross tests such as salt fog and alternate salt-immersion tests with their lack of quantitative values for corrosivity or relative corrosivity and no direct relationship to service experience. Atmospheric outdoor tests where panels are exposed to various environments require a time scale which precludes rapid materials-selection decisions or paint-protection measure evaluations. These tests are limited to specific environments and seldom take into account stress factors which may accelerate the localized corrosion and enhance crack growth leading to premature failure. Cyclic loading is, of course, also precluded. Establishing realistic test environments requires, at a minimum, a reasonable selection of atmospheric environmental variables coupled with stress factors which aerospace components are expected to experience. The selection of appropriate air-quality standards is difficult and should be based upon knowledge of ambient-air pollutant levels and experimental work to determine the relative importance of these pollutants. The effects of SO_2 for high-strength steels and NO_2 for high-strength aluminum alloys must be related to the interaction of these gases with water vapor and airborne particulates and to causal factors. In this paper, the design and layout of the experimental apparatus for simulating the environment and the initial results obtained in environmentally accelerated crack-growth studies conducted on high-strength steels and aluminum alloys are given. Experiments have been conducted in dry and humid air and then in more aggressive environments containing a mixture of SO_2 and humid air. Rising-load tests have been used to determine the apparent K_{ISCC} for 4340 steels and high-strength aluminum alloys in these environments. Fractographic analysis has been employed to correlate the results and the types of failure that have occurred.

EXPERIMENTAL

Materials

A 50.8-mm-thick plate of 4340 steel of aircraft quality obtained from Jorgensen Steel was used. The steel was heat treated to yield strengths of 1240, 1345, and 1440 MPa. The high-strength Al 7075-T6 alloy with a yield strength of 440 MPa was obtained from Rockwell International in the form a 76.2-mm-thick plate. Research-grade SO_2 and N_2 were employed. Distilled water was used throughout the experiments.

The critical stress-intensity factor, K_{IC}, the threshold stress intensity for stress-corrosion cracking, K_{ISCC}, and crack-growth data were obtained using compact-tension plane-strain fracture-toughness specimens as shown in Fig. 1. Both steel and aluminum specimens were machined in the short-transverse (ST) orientation.

All fractured surfaces were examined visually and then by light microscopy. The specimens were then ultrasonically cleaned in acetone, deionized water, and methyl alcohol. The light-microscopic observation was followed by scanning electron microscopy (SEM) for detailed examination of the fractured surfaces.

Test Methods

For fracture-toughness determinations the compact-tension specimens were precracked to 2.54 mm by fatigue cracking according to ASTM specifications. Two specimens from each heat treatment were loaded monotonically to failure to determine the stress intensity at fracture, K_{IC}.

The apparent threshold for sustained-load stress-corrosion cracking, K_{ISCC}, in humid air and in different mixtures of humid air and SO_2 was estimated using the accelerated rising-load procedure [4]. The testing technique utilized was identical to the procedure used for K_{IC} fracture-toughness testing (ASTM Test for Plane-Strain Fracture Toughness of Metallic Materials E 399-72) [5], except that a slower rate of loading was employed and the specimen was exposed to the environment while being loaded. These tests were conducted with standard 19.05-mm-thick compact-tension specimens. The specimens were precracked to crack lengths of 2.54 mm at stress intensities below 15 MPa $\sqrt{m}$ for steel and 7 MPa $\sqrt{m}$ for Al 7075-T6 (R - 0.1 and f - 0.1 Hz). A special environmental chamber (to be described in detail later) was used to maintain and control the constituents of the specific environments required for the tests. The specimens were loaded in air, in 80% relative humidity, in 1000 ppm SO_2 + 80% RH, and in 1000 ppm SO_2 + 100% RH, at fixed loading rates corresponding to 5, 22, and 88 N/min. K_{ISCC} values were estimated from the load-displacement record, using the five-percent secant offset procedure similar to that used for the K_{IC} testing [5]. The results are given in Tables I and II.

All corrosion-fatigue tests were conducted at room temperature using a 100 KN Materials Testing System (MTS) machine. The crack length was monitored through crack-opening-displacement (COD) measurements during fatigue testing. To determine the crack length from COD data, compliance measurements were carried out for both high-strength steels and aluminum alloys. Tests were conducted in air, and crack lengths were determined using optical and COD measurements simultaneously on the MTS machine. The COD was measured by a double-cantilever displacement gauge prepared in accordance with the ASTM designation [5]. The displacement gauge was calibrated to measure COD from 0 to 1.25 mm ± 0.0125 mm using a Daytronic strain-gauge amplifier. The COD was recorded as a function of cycles.

A sinusoidal tension-tension waveform was employed for all fatigue-crack-growth-rate tests. Most of the tests were conducted at an R ratio (K_{min}/K_{max}) of 0.6 and a frequency of 0.1 Hz. The slow frequency and high R ratio were utilized

to facilitate the observation of environmental effects. Limited tests were conducted at frequencies of 0.25 and 0.5 Hz also. All specimens were initially precracked according to ASTM specification E 399-72 [5] on the same MTS machine on which the corrosion-fatigue tests were conducted.

No significant differences were found in the COD/load and crack length/load curves. The crack length, a, was calculated from the analytical compliance relationship [6]

$$a/W = 1.001 - 4.6695\ U + 18.460\ U^2 - 236.82\ U^3 + 1214.94\ U^4 - 2143.6\ U^5$$

where

$$U = \frac{1}{\sqrt{\frac{EB\ (COD_{Max} - COD_{min})}{P_{Max} - P_{Min}} + 1}}$$

E is the Young's modulus and P the stress. W and B are the dimensions indicated in Fig. 1. The stress-intensity values were calculated from [6]

$$K = \frac{P}{BW^{1/2}} \frac{(2 + a/w)[(0.886 + 4.64(a/w)] - 13.32(a/w)^2 + 14.72(a/w)^3 - 5.6(a/w)^4}{(1 - a/w)^{3/2}}$$

where B and W are the dimensions indicated in Fig. 1 such that B and a > 2.5 $(K_{IC}/YS)^2$, with K_{IC} being the fracture toughness and YS is the tensile yield strength. The crack-length-versus-number-of-cycles data were converted to fatigue-crack-growth rates (da/dN) using a computer program [6]. Seven to eleven data points were fitted to a second-order polynomial, and the derivative (da/dN) was then obtained for the middle data point. This process was then repeated over the entire range of data.

Controlled-Atmosphere Environmental Chamber

The environmental chamber and the gas-train assembly are shown in Fig. 2. The chamber is made of 316 stainless steel while the grips, pull rods, and pins are made of 17-4 PH steel which exhibits good resistance to wet SO_2 and wet NO_2 environments. It is a leak-proof system with bellows and other attachments to attain high vacuum. The temperature inside can be controlled from 0 to 1000°F. The unit is installed in a closed-loop MTS machine for conducting mechanical tests in simulated realistic environments.

The test atmospheres were supplied through the gas train which consists of a gas mixing and delivery system. High-purity bottled gases (SO_2 and dry air in this case) were metered by Matheson flowmeters 601 and 603 and then mixed in the mixing tube. The concentration of SO_2 in the chamber is routinely measured by calibrated Gastec analyzer tubes. Special gas-sampling outlets are provided in the chamber. The relative humidity (RH) inside the chamber is controlled by means of a BMA dry and wet bulb hygrometer. The water vapor is added in the form of steam by boiling distilled water in a flask maintained at a constant temperature. The steam flow is controlled by the output voltage of the BMA controller which monitors the opening and closing of the solenoid valve on the steam line. The steam is injected into the gas mixture prior to its entry into the chamber in order to obtain the required mixture of SO_2 and RH air.

Gas pressures used in all the tests have been slightly above atmospheric to provide positive flow through the environmental chamber. The gas inlet and outlet are positioned specifically to minimize the channeling effect. The gas is circulated inside the chamber by means of a circulating fan (placed inside the chamber) to maintain a uniform environment throughout the chamber. Negligible condensation occurred during these tests except in the case of 100% RH. The fatigue-crack-propagation data previously discussed were obtained using compact-tension plane-strain fracture-toughness specimens (Fig. 1). Tests were conducted in the controlled atmosphere inside the environmental chamber as described. The inert dry nitrogen was used as a control, while the 80% RH air, 1000 ppm SO_2 + 80% RH, and 1000 ppm SO_2 + 100% RH were used as representative aggressive environments for stress corrosion and environmentally accelerated corrosion fatigue.

RESULTS AND DISCUSSION

Crack Propagation

The fatigue-crack-propagation behavior of many ferrous and nonferrous alloys can be schematically represented as in Fig. 3 [8]. The rate of crack growth depends strongly upon K at K levels approaching K_C or K_{IC} at the high end and at levels approaching an apparent threshold at the low end, with an intermediate region that depends upon some power of K or ΔK. The upper end corresponds to the onset of unstable fracture, while the lower end corresponds to the fatigue "threshold" ΔK_{th} [9,10] which appears to be related to the metallurgical structure [11].

The environment-enhanced fatigue-crack-growth response of high-strength metals may be broadly characterized in terms of three general patterns of behavior [12], as illustrated schematically in Fig. 4. The first type of behavior represents those material-environment systems where fatigue-crack-growth rates are enhanced by the presence of an aggressive environment through a synergistic action of corrosion and cyclic loading. This is "below K_{ISCC}" behavior [13-15] and applies to materials which are not susceptible to stress corrosion where $K_{ISCC} > K_{IC}$. This behavior is classified as true corrosion fatigue. The second type of behavior is representative of those systems where there is a substantial environment-enhanced sustained-load crack-growth component [16,17] which occurs whenever the stress intensity in the cycle is above K_{ISCC}. This behavior is classified as stress-corrosion fatigue. The most common type of behavior pertains to material/environment systems which exhibit stress-corrosion fatigue above K_{ISCC} and also true corrosion fatigue at all stress-intensity levels. Such behavior lies between the two extremes and is shown in Fig. 4(c).

Crack Growth Behavior of Al 7075-T6 and 4340 Steel

The accelerated atmospheric effects resulting from the variation of the relative humidity upon observed crack-growth rates were investigated. The low-cycle corrosion-fatigue data are expressed in terms of crack-growth rate da/dN as a function of the stress-intensity-factor range ΔK. The dependence of crack-growth rate upon the humidity level in air for Al 7075-T6 is shown in Fig. 5. At high levels of humidity such as 80% RH, the crack-growth rates were substantially increased as compared to those in dry air ($\leq$ 5% RH). The immersion results for crack growth in aqueous solutions are shown for the sake of comparison. While increasing relative humidity also increases the crack-growth rates,

the change in crack-growth rate from gaseous environment to total-immersion aqueous environment is much more significant. This rate is also less realistic for estimating corrosion reactions except where standing water is present. Similar results on several aluminum alloys have been obtained by other workers [18-25]. The commonly accepted explanation of crack-growth acceleration due to a high level of humidity is the pressure mechanism of hydrogen embrittlement suggested by Broom and Nicholson [19] which requires a water-metal surface reaction and proposes that the increase in the rate of fatigue-crack growth results from the synergistic action of a mechanical process--fatigue, which creates a sufficient amount of fresh surface--and the chemical reaction of water vapor with the resulting fresh surface.

Figure 6 represents the crack-growth-rate data on 4340 steel with a yield strength of 1345 MPa obtained at three levels of humidity. In all these tests a frequency of 0.1 Hz and a load ratio R of 0.1 were used. While the shapes of the three curves are similar, noticeable differences exist in the crack-growth rates at high K levels. Note that although the differences in crack-growth rates (at different humidity levels) are small, very definite differences are present. The differences found are reproducible within an experimental error of da/dN less than the Δda/dN values. Similar differences in crack-growth rates were observed for Al 7075-T6. These differences become more pronounced when one considers data on cycles to failure. These data are shown in Table III for both Al 7075-T6 and 4340 steel. Similar increases in crack-growth rates of high-strength 4340 steel due to water vapor were observed under both sustained and cyclic loading by Lynch and other workers [26-32]. Dahlberg [33] has demonstrated more distinct differences in the crack-growth rates of 4340 steel tested at different humidity levels when an R ratio of 0.8 was used. However, the differences in crack-growth rates with increasing humidity levels were similar to those obtained in the present investigation where smaller R ratios were used.

Although several mechanisms have been suggested for hydrogen embrittlement [34-37] (such as the decohesion model [36] and the pressure model [37]), no single theory gives a complete description of the problem. For high-strength steels, however, in "hydrogen-producing" atmospheres (e.g., H_2, H_2O, H_2S), decohesion theories are widely accepted [38-41, 37] (for monotonic and cyclic loading). Also the general concensus is that the presence of water vapor in the atmosphere enhances crack-growth rates for both high-strength aluminum alloys and steels.

Crack Propagation of Al 7075-T6 and 4340 steel in humid SO_2

The corrosion-fatigue tests with high-strength aluminum alloys were extended to more aggressive environments of a mixture of 80% RH and 1000 ppm SO_2. Two sets of tests using stress ratios of 0.6 (R = 0.6) and 0.8 (R = 0.8) were conducted with frequencies ranging from 0.1 to 1 Hz. The crack-growth results for R = 0.6 are shown in Fig. 7, while Fig. 8 shows the da/dN-vs-ΔK plot for a stress ratio of 0.8. Frequency has very little effect from 0.1 to 0.5 Hz at both stress ratios, but there is a surprising difference in the behavior at 1 Hz. At a stress ratio of 0.6, and a frequency of 1 Hz, crack-growth rates decrease at higher K-values compared to the rates obtained at frequencies of 0.1 and 0.5, while the crack-growth rates are almost the same at these higher

K-levels for all three frequencies at a stress ratio of 0.1. However, the rates are comparatively higher at lower K-levels, at a frequency of 1 Hz. There is no easy explanation for such behavior, and more tests must be conducted to clearly define such differences in behavior. However, the effect of stress ratio is more distinct than that of frequency. At a stress ratio R = 0.6, the da/dN-vs-ΔK curve has a more pronounced intermediate or second region, while there is little evidence of a normal intermediate region (as shown in Fig. 8) at a stress ratio R = 0.8, except at a frequency of 1 Hz. This difference in the intermediate region of the da/dN-vs-ΔK curve has been reported to be stress-ratio and frequency dependent [24,42].

It appears that there is a near plateau region followed by a maximum in the da/dN-vs-ΔK curves obtained at a stress ratio of 0.6, but it is not very well defined, in contrast to the case of 1440 MPa steel. Hence, no attempt was made to determine K_{ISCC} from a similar extrapolation as has been done in the case of 1440 MPa steel. The K_{ISCC} values in humid SO_2 were determined by the rising-load method; the results are shown in Table I. The difference in the K_{IC} value and the apparent K_{ISCC} value was not very great. This leads to the conclusion that either the rising-load test for determination of K_{ISCC} does not hold sufficiently for this material-environment system or the humid SO_2 atmosphere has a small and insignificant embrittling effect upon Al 7075-T6 at a strength level of 440 MPa. This contrasts markedly with the results for 4340 steel.

High-strength 4340 steel at yield strengths of 1240 MPa and 1440 MPa was tested at a load ratio of 0.6 and a frequency of 0.1 Hz. The atmospheres were ambient air, dry nitrogen, 80% RH air, and 1000 ppm SO_2 in 80% RH air. The crack-growth results for 1240 MPa steel are shown in Fig. 9, while Fig. 10 shows the da/dN-vs-ΔK plot for 1440 MPa steel. A comparison of these two figures shows that there is a greater enhancement in the crack-growth rates for 1440 MPa steel as compared to 1240 MPa steel due to the SO_2 environment. These data show a plateau intermediate region followed by a maximum of the da/dN-vs-ΔK plot obtained for 1440 MPa steel tested in the 1000 ppm SO_2 + 80% RH environment. A similar, but less-pronounced maximum is obtained for 1240 MPa in this same environment. The ambient air and 80% RH plots, however, follow the normal trend [8]. This difference in the nature of the plot (or appearance of a plateau followed by a maximum) is expected when the K level exceeds the K_{ISCC} value for the metal-environment system. In general, this follows the trend of Fig. 4(c) which is most significant because the extrapolation from this slope change to the abscissa of the plot produces the K_{ISCC} value as shown in Fig. 4(c). Accordingly, the K_{ISCC} values have been obtained from Figs. 9 and 10 and are 55 and 46 MPa $\sqrt{m}$ for 1240 MPa and for 1440 MPa steels. The accuracy of this estimate has been further verified by the rising-load method and fractographic observations. The K_{ISCC} value obtained from 1440 MPa steel by such extrapolation is in very close agreement with the K_{ISCC} values obtained from the other observations. The high value of K_{ISCC} obtained for 1240 MPa steel could not be supported by either rising-load or fractographic observations. Such high values of K_{ISCC} obtained by extrapolation of da/dN-vs-ΔK curves have been reported previously [43]. However, the K_{ISCC} value obtained by such extrapolation for 1440 MPa steel is quite consistent and accurate. The validity of this extrapolation is supported by the results of Austen, et al. [44], on high-strength 835M30 steel in a 3.5% NaCl environment. However, the high value of K_{ISCC} obtained for 1240 MPa steel requires further studies in several environments. A more detailed investigation of the nature of the da/dN-vs-ΔK plot is required when there is a very small

difference in K_{ISCC} and K_C values for the metal-environment system. In this case 1240 MPa steel is not so susceptible as 1440 MPa steel to hydrogen-assisted stress-corrosion cracking in the environmental conditions of the test, and the results apparently are intermediate between the first two cases of the schematic presentation of Fig. 4. In such a case, further detailed study of frequency/load/R ratio effects may be necessary to improve the determination of K_{ISCC} by extrapolation.

Modified Rising-Load K_{ISCC} Tests

The approximate values of K_{ISCC} obtained for 1240 MPa and 1440 MPa steels in various environments are shown in Table I. Only two loading rates of 22 and 88 N/min were used. The values quoted in Table I must be taken as the higher-limit estimates because of the rapid K rates utilized and the limited nature of the test procedure. More experiments at slower rates should improve the approximation of K_{ISCC} values. The K_{ISCC} values for Al 7075-T6 were estimated by a modified step-by-step loading practice. The schematics of the procedure are shown in Fig. 11. The results are given in Table II.

Fractographic Analyses

Fractographic analyses of the fracture surfaces of the specimens were conducted to provide further information concerning the crack-tip mechanism in corrosion fatigue of 4340 steels at different K levels in humid SO_2 environments. The fracture features of Al 7075-T6 fatigued in humid SO_2 will be reported in a later paper.

Figure 12 shows fractographs taken from the surface of a 1240 MPa steel specimen tested in 1000 ppm SO_2 + 80% RH. These fractographs indicate that at low values of K, 40.5 MPa $\sqrt{m}$, the surface features are very ductile [Fig. 12(a)]. At higher values of K, there is little evidence of intergranular fracture. The fracture is mainly transgranular and ductile in nature. No substantial component of intergranular fracture could be found, even in the fracture zone corresponding to high values of K, $\approx$ 57.5 MPa $\sqrt{m}$ (near the fast fracture) [Fig. 12(b)]. Different fracture-surface characteristics were obtained for 1440 MPa steel corrosion fatigued in 1000 ppm SO_2 + 80% RH.

Figure 13(a) shows the ductile nature of failure at low K values of 35 - 36 MPa $\sqrt{m}$, while Fig. 13(b) shows the mixed mode of failure, corresponding to a K value of $\approx$ 40 MPa $\sqrt{m}$. Figure 13(c) is a typical fractograph obtained in the fracture zone corresponding to a K value of $\approx$ 46 MPa $\sqrt{m}$. The entire fractured surface was scanned several times, and a definite intergranular failure mechanism was observed over the entire cross section when the K value exceeded 45 - 46 MPa $\sqrt{m}$. The value of K_{ISCC} was approximated by careful measurement of the crack length and found to be $\approx$ 46 MPa $\sqrt{m}$, which is in agreement with the K_{ISCC} value obtained from the da/dN-vs-ΔK plot; this value falls within good approximation of the value obtained by the rising-load method.

Figure 14 shows the fractographs obtained from the fractured surface of 1240 MPa steel tested in dry N_2, which are shown for comparison. The fractured surfaces [Fig. 14(a)] are characteristic of ductile failure, containing dimpled rupture. In Fig. 14(b) the dimples can be more clearly seen at higher magnification.

CONCLUSIONS

The presence of water vapor in the atmosphere accelerates the crack-growth rates of high-strength steels and aluminum alloys. Crack-growth rates increase with increasing relative humidity, with the effect being more pronounced in steel at a yield strength of 1440 MPa as compared to 1240 MPa.

There is a significant increase in crack-growth rates (and corresponding decrease in cycles to failure) for high-strength alloys in full immersion to aqueous solutions as compared to 100% RH air atmosphere.

Corrosion-fatigue crack-growth rates increase from ambient air to 80% RH air to 80% RH air + 1000 ppm SO_2. This is true for all alloys, with the effects being more pronounced in the 1440 MPa steel than in the 1240 MPa steel.

The value of K_{ISCC} can be extrapolated from the corrosion-fatigue curve, providing the conditions of load, frequency, and R ratio are optimized. The results of rising-load corrosion-fatigue extrapolation and fractography experiments are in excellent agreement for the 1440 MPa steel. Thus, a rapid determination of K_{ISCC} is provided for susceptible alloys. For aluminum the embrittling effect in high humidity and SO_2 atmosphere is insufficient to obtain an accurate K_{ISCC} value from the corrosion-fatigue curve.

ACKNOWLEDGMENTS

The authors express their thanks to F. M. Thornton for reducing the experimental data and to M. B. Strope for assisting in the fractographic analysis.

REFERENCES

1. L. H. Bennett, J. Kruger, R. L. Parker, E. Passaglia, C. Reimann, A. W. Ruff, and H Yakowitz, Economic Effects of Metallic Corrosion in the United States, Parts I and II, NBS Special Publication 511-1,2 (U. S. Department of Commerce, National Bureau of Standards, Washington, D.C., May 1978).

2. M. Hoch and J. Gwinn (eds.), Proceedings of the AFOSR/AFML Corrosion Workshop, AFML-TR-77-175 (Air Force Materials Laboratory, Wright-Patterson Air Force Base, OH, 1975).

3. E. D. Verink, Jr. (ed.), AFOSR/AFML Workshop on Corrosion of Aircraft (St. Augustine, FL, September 13-15, 1977) (The University of Florida, Gainsville, FL, 1977).

4. W. G. Clark and J. D. Landes, Stress Corrosion - New Approaches, ASTM STP 610 (American Society for Testing and Materials, Philadelphia, PA, 1976), p. 108.

5. ASTM E399-72, Standard Test for Plane-Strain Fracture Toughness of Metallic Materials, 1972 Annual Book of ASTM Standards (American Society for Testing and Materials, Philadelphia, PA, 1972).

6. N. E. Ashbaugh, Technical Report AFML-TR-79-4127 (Air Force Materials Laboratory, Wright-Patterson Air Force Base, OH, September 1979).

7. ASTM E647-78T, Tentative Test Method for Constant-Load-Amplitude Fatigue Crack Growth Rates Above 10^{-8} m/cycle, 1978 Annual Book of ASTM Standards (American Society for Testing and Materials, Philadelphia, PA, 1978).

8. B. F. Brown (ed.), Stress Corrosion Cracking in High Strength Steels and in Titanium and Aluminum Alloys (U. S. Government Printing Office, Washington, D.C., 1972).

9. P. C. Paris, "Testing for Very Slow Growth of Fatigue Cracks," MTS Closed Loop Magazine 2(5) (1970).

10. R. J. Bucci, W. G. Clark, Jr., and P. C. Paris, in Stress Analysis and Growth of Cracks, ASTM STP 513 (American Society for Testing and Materials, Philadelphia, PA, 1972), p. 177.

11. J. A. McMillan and R. P. Wei, Met. Trans. 1, 1741 (1970).

12. A. J. McEvily and R. P. Wei, "Fracture Mechanics and Corrosion Fatigue," in Proc. Int. Conf. on Corrosion Fatigue - Chemistry, Mechanics and Microstructures (Storrs, CT, 1972) (National Association of Corrosion Engineers, Houston, TX, 1972), p. 381.

13. J. M. Barsom, "Corrosion Fatigue Crack Propagation Below K_{ISCC}," Eng. Fract. Mech. 3, 15 (1971).

14. J. P. Gallagher, "Corrosion Fatigue Crack Growth Rate Behavior Above and Below K_{ISCC}," J. Materials 6, 941 (1971).

15. J. P. Gallagher and R. P. Wei, "Corrosion Fatigue Crack Propagation in Steels," in Proc. Int. Conf. on Corrosion Fatigue - Chemistry, Mechanics and Microstructure (Storrs, CT, 1972) (National Association of Corrosion Engineers, Houston, TX, 1972), p. 409.

16. R. P. Wei. J. Eng. Fract. Mech. 1, 633 (1970).

17. R. P. Wei and J. D. Landes, Mat. Res. and Std. ASTM 9, 25 (July 1969).

18. N. J. Wadsworth, A. Nicholson, and J. Hutchins, "The Effect of Atmospheric Corrosion on Metal Fatigue," Phil. Mag. 3, 1154 (1958).

19. T. Broom and A. Nicholson, "Atmospheric Corrosion Fatigue of Age Hardened Aluminum Alloys," J. Inst. Met. 89, 183 (1960-1).

20. F. J. Bradshaw and C. Wheeler, Appl. Mat. Res. 5, 112 (1966).

21. A. Hartman, Int. J. Fract. Mech. 4, 167 (1965).

22. R. P. Wei, Int. J. Fract. Mech. 4, 159 (1968).

23. R. P. Wei and J. D. Landes, Int. J. Fract. Mech. 5, 69 (1969).

24. A. Hartman and J. Schijve, Eng. Fract. Mech. 1, 615 (1970).

25. W. P. Wei, et al., "Fracture Mechanics and Surface Studies of Fatigue Crack Growth in Al Alloys," Report 9 (IFSM-79-98) (Lehigh University, Bethleham, PA, April 1979) (Contract N00014-75-C-0543).

26. C. T. Lynch, F. W. Vahldiek, and F. W. Thornton, in Proceedings of the 1978 Tri-Service Conference on Corrosion (October 4-6, 1978, New Orleans, LA).

27. P. M. Che-Yu Li, P. M. Talda, and R. P. Wei, Int. J. Fract. Mech. 3, 29 (1967).

28. H. H. Johnson and A. M. Willner, Appl. Mat. Res. 4, 34 (1965).

29. G. G. Hancock and H. H. Johnson, Trans. Met. Soc. AIME (April 1966).

30. G. L. Hanna, A. R. Troiano, and E. A. Steigerwald, Trans. ASM 57, 658 (1968).

31. W. A. van der Sluys, Trans. ASME 89D, 28 (1967).

32. J. P. Gallagher, "Environmentally Assisted Fatigue Crack Growth Rates in SAE 4340 Steel, "Ph.D. Dissertation (Dept. of Theoretical and Applied Mechanics, Univ. of Illinois, Urbana, IL, 1968).

33. E. P. Dahlberg, Trans. ASM 58, 46 (1965).

34. H. H. Johnson and P. C. Paris, Eng. Fract. Mech. 1, 3 (1968).

35. H. H. Johnson, "On Hydrogen Brittleness in High Strength Steels," in Proc. Conf. Fundamental Aspects of Stress Corrosion Cracking (Ohio State University, Columbus, OH, 1967).

36. R. A. Oriani and P. H. Josephic, Acta. Met. 22, 1065 (1974).

37. C. Zappfe and C. Sims, Trans. AIME 145, 225 (1941).

38. A. W. Thompson and I. M. Bernstein, in Advances in Corrosion Science and Technology (R. W. Staehle and M. G. Fontana, eds.), Vol. 7 (Plenum Press, NY, 1973).

39. R. P. Wei and J. D. Landes, Mat. Res. Stds. 9, 25 (1969).

40. I. M. Austen and P. McIntyre, Met. Sci. 13, 420 (1979).

41. R. O. Ritchie, M. H. Castrocedeno, V. F. Zackay, and E. R. Parker, Met. Trans. A. 9A, 35 (1978).

42. K. Walker, in ASTM STP 462 (American Society for Testing and Materials, Philadelphia, PA, 1970), pp. 1-14.

43. R. O. Ritchie, S. Suresh, and J. Toplosky, M.I.T. Fatigue and Plasticity Lab Report No. FPL/R/80/1030 (Massachusetts Institute of Technology, Cambridge, MA, January 1980) (Contract DE-AC02-79ER10389,A000).

44. I. M. Austen and E. F. Walter, "Quantitative Understanding of the Effects of Mechanical and Environmental Variables on Corrosion Fatigue Crack Growth Behavior," in Proceedings Int. Conf. Effect of Environment on Fatigue (Institute of Mechanical Engineers, London, 1977), pp. 1-10.

TABLE I

APPARENT K_{ISCC} VALUES OBTAINED BY RISING LOAD TESTS

SPECIMEN #	ENVIRONMENT	LOADING RATE N/min	*APPARENT K_{ISCC} MPa $\sqrt{m}$	YIELD STRENGTH MPa
2B	1000ppm SO_2 + 80% RH	22	55	1440
3B	1000ppm SO_2 + 80% RH	88	49	1440
10A	1000ppm SO_2 + 80% RH	22	72	1240
23A	1000ppm SO_2 + 100% RH	22	70	1240
29A	80% RH	22	78	1240
15A	50% RH	22	78	1240

* THESE VALUES ARE APPROXIMATE.

TABLE II

APPARENT K_{ISCC} VALUES OBTAINED FROM RISING LOAD TEST

SPECIMEN	ENVIRONMENTAL	LOADING RATE (N/MIN.)	HOLD TIME	APPARENT K_{ISCC} OR K_{IC} (MPa)
STA-36	80% RH	88	TO FAILURE	165.3
STA-33	80% RH	88	80 MPa FOR 24 HR.	
		22	90 MPa FOR 24 HR.	
		22	105 MPa FOR 24 HR.	
		22	110 MPa FOR 100 HR.	
		22	TO FAILURE	177.8
STA-1	1000 PPM SO_2 + 80% RH	88	TO FAILURE	175.2
STA-24	1000 PPM SO_2 + 80% RH	88	125 MPa FOR 24 HR.	
		22	134 MPa FOR 50 HR.	
		22	142 MPa FOR 50 HR.	
		22	TO FAILURE	150.0

TABLE III

SPECIMEN LIFE IN CYCLES

4340 STEEL 1335 MPa		
SPECIMEN #	RH	N_f (cycle)
1	DRY AIR ≤5 %	60,174
2	65%	40,593
3	100%	33,864
Al 7075-T651		
SPECIMEN #	RH	N_f (cycle)
1	DRY AIR ≤ 5%	40,347
2	80%	26,950
3	100%	41,005

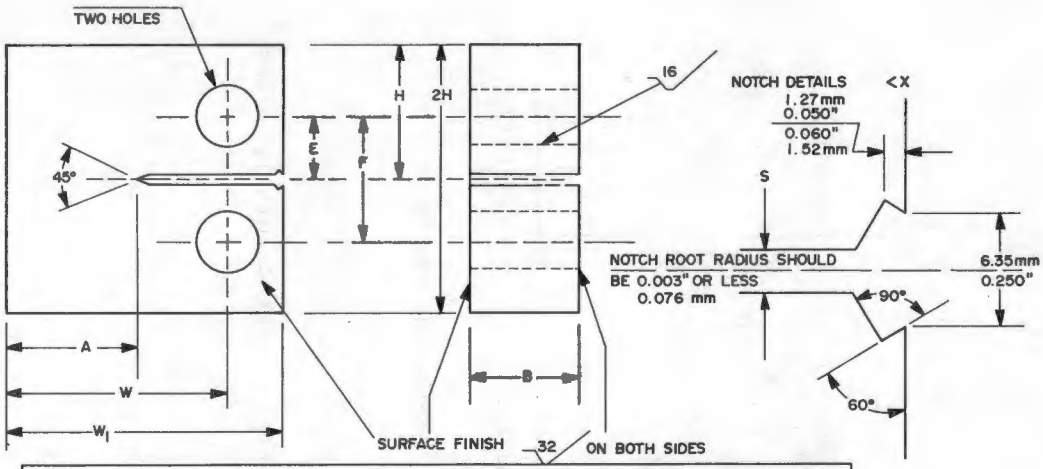

MATERIAL	B	A	W	W_1	S	E	F	H	D
ALUMINUM	25.4mm	29.2mm	50.8mm	63.5mm	2.36mm	13.97mm	27.94mm	30.48mm	12.7mm
STEEL	19.05mm	22.22mm	38.10mm	47.62mm	1.90mm	10.46mm	20.95mm	22.86mm	9.52mm

Figure 1. Compact-Tension Specimen.

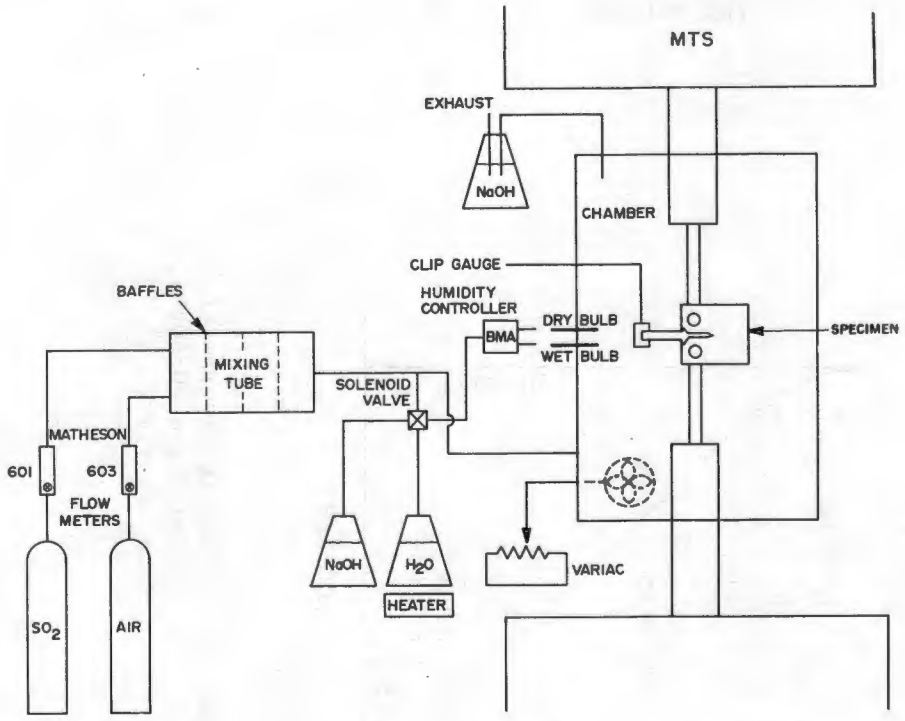

Figure 2. Gas Train and Environmental Chamber.

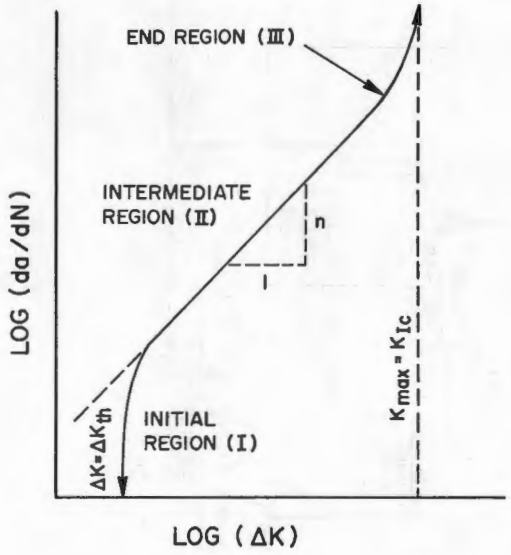

Figure 3. Schematic Diagram of Fatigue-Crack-Growth-Rate Behavior.

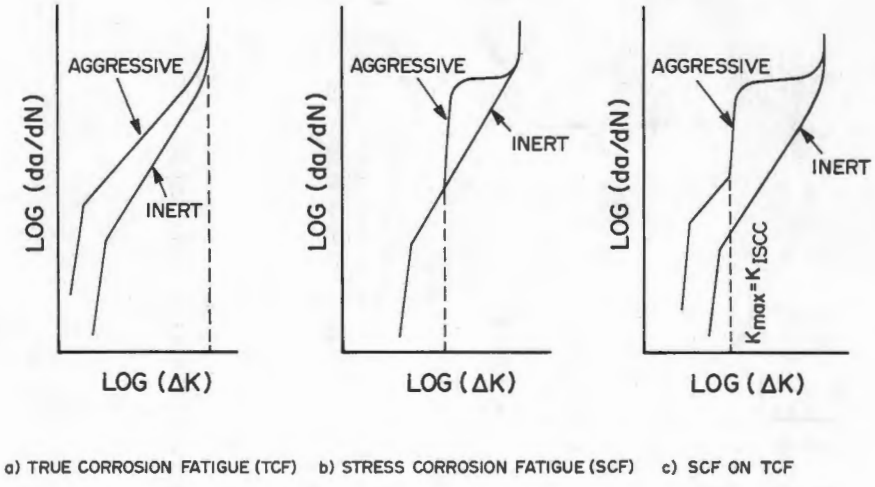

Figure 4. Types of Fatigue-Crack-Growth Behavior.

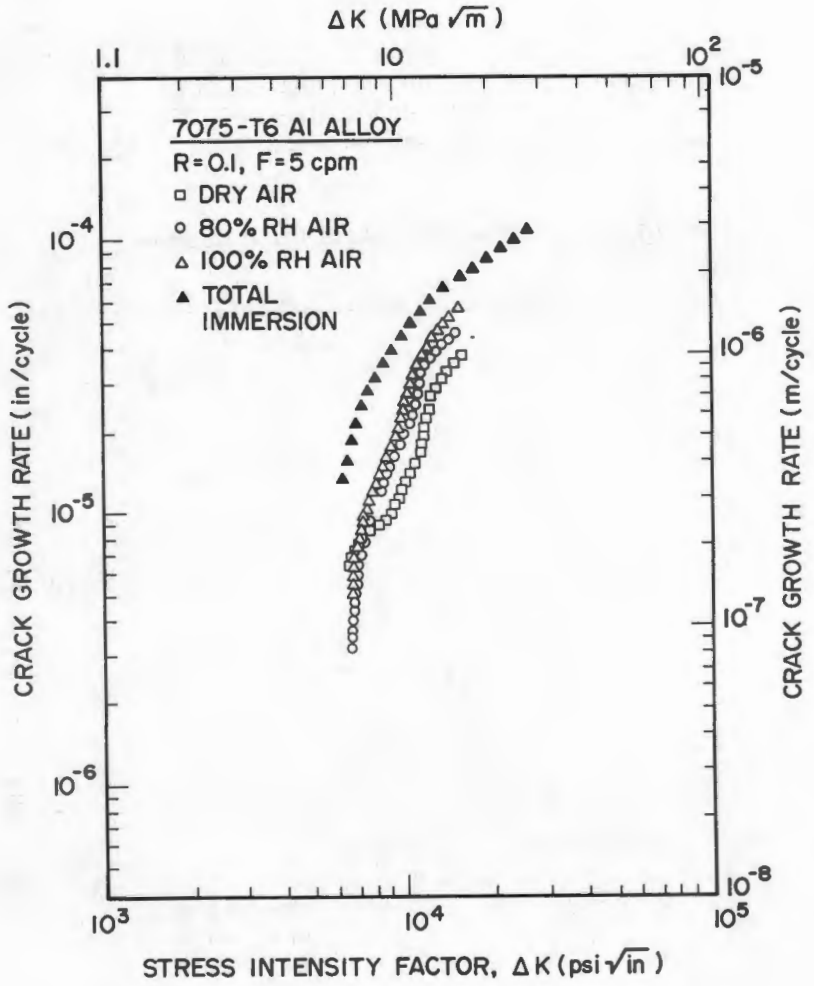

Figure 5. Crack-Growth Rate Data Obtained for Al 7075-T6 Tested at Various RH Levels.

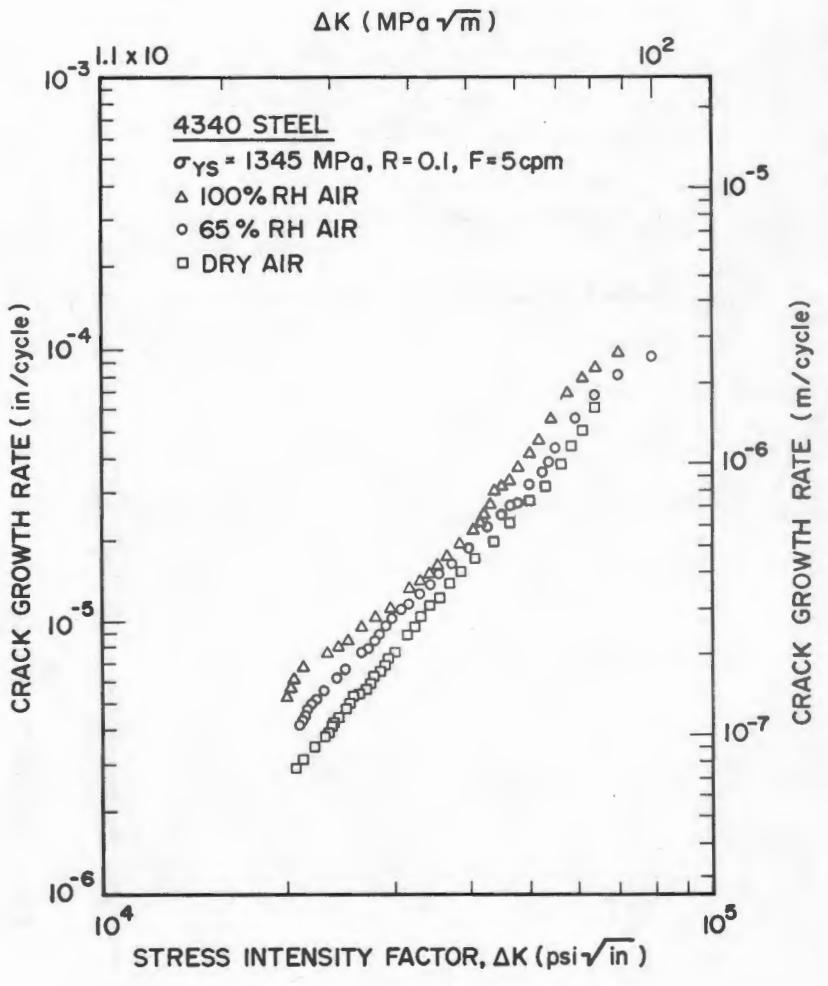

Figure 6. Crack-Growth-Rate Data Obtained for 4340 Steel (1345 MPa) Tested at Various RH Levels.

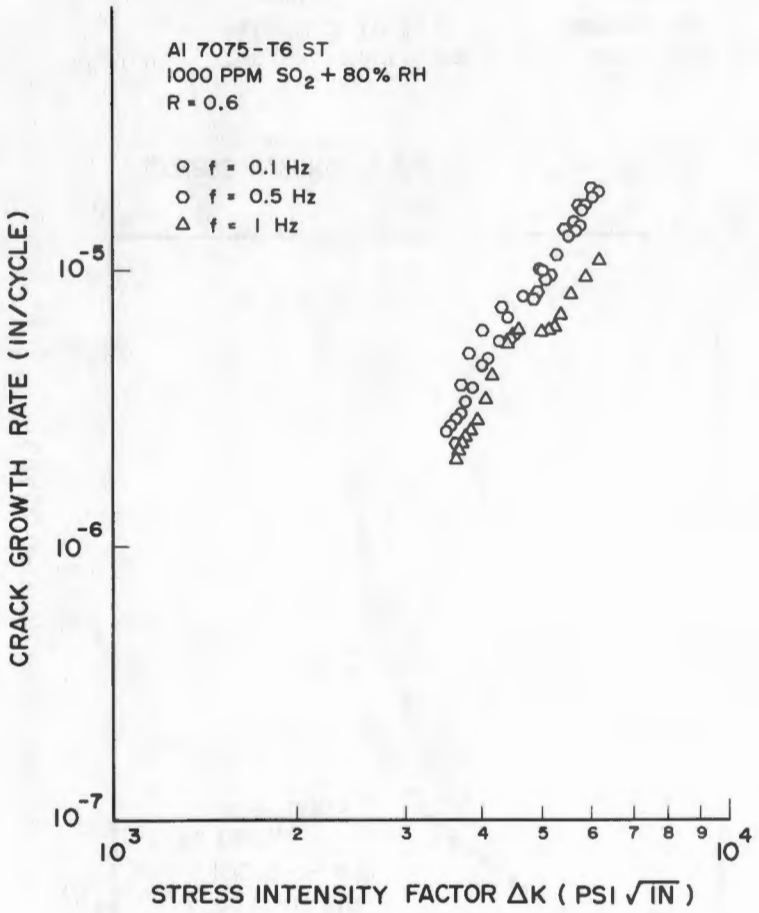

Figure 7. Crack-Growth-Rate Data Obtained for Al 7075-T6 Tested in 1000 ppm SO_2 + 80% RH Environment at a Stress Ratio of 0.6.

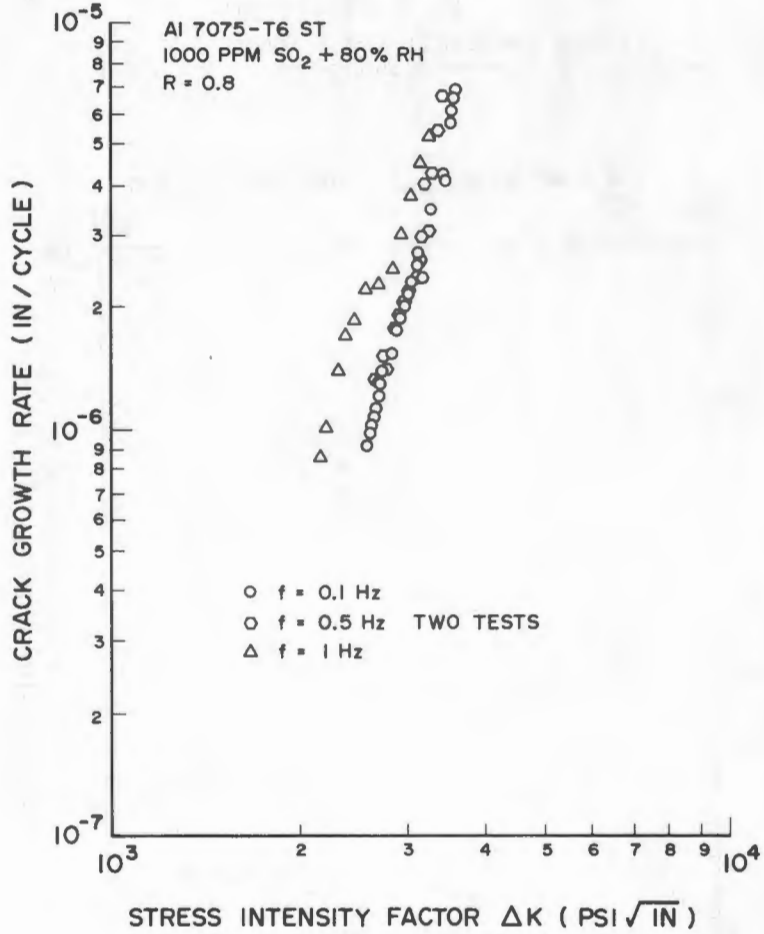

Figure 8. Crack-Growth-Rate Data Obtained for Al 7075-T6 Tested in 1000 ppm SO_2 + 80% RH Environment at a Stress Ratio of 0.8.

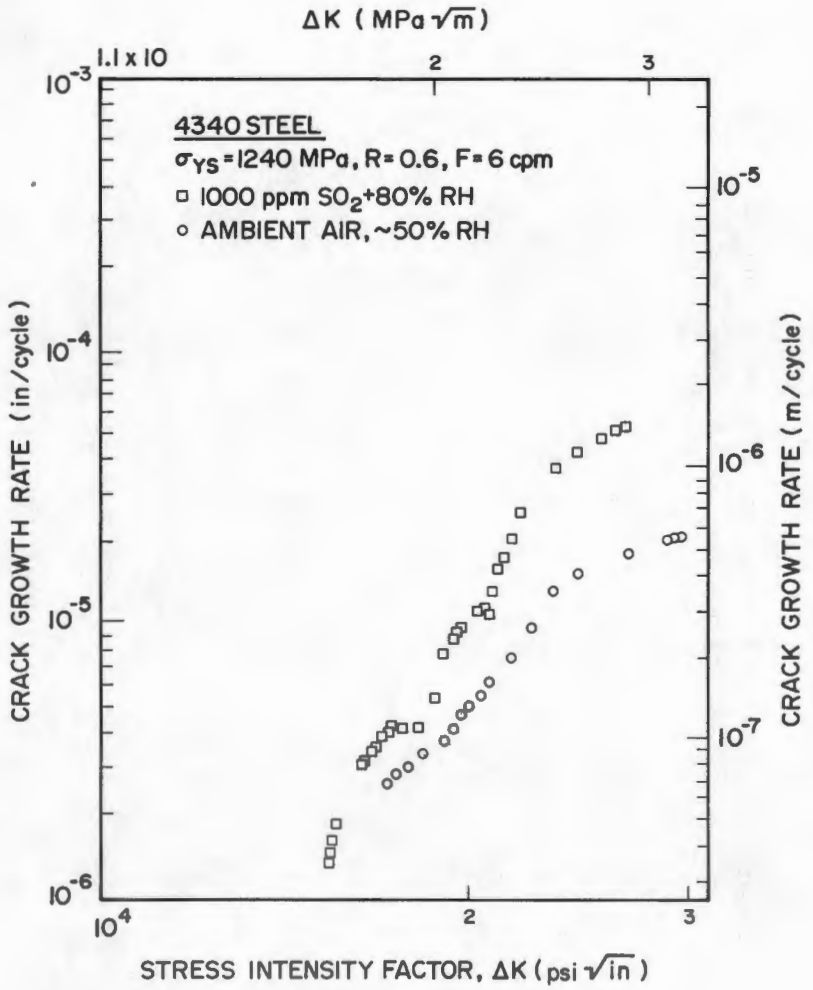

Figure 9. Crack-Growth-Rate Data Obtained for 4340 Steel (1240 MPa) Tested in 1000 ppm SO_2 + 80% RH Environment.

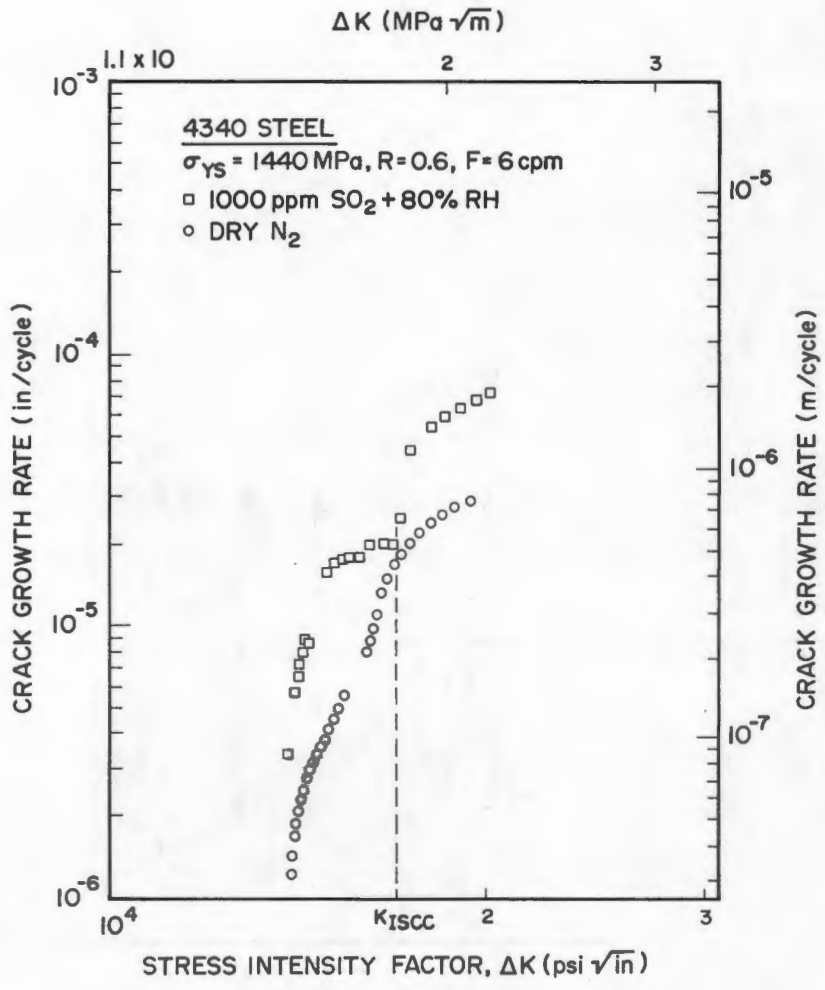

Figure 10. Crack-Growth-Rate Data Obtained for 4340 Steel (1440 MPa) Tested in 1000 ppm SO_2 + 80% RH Environment.

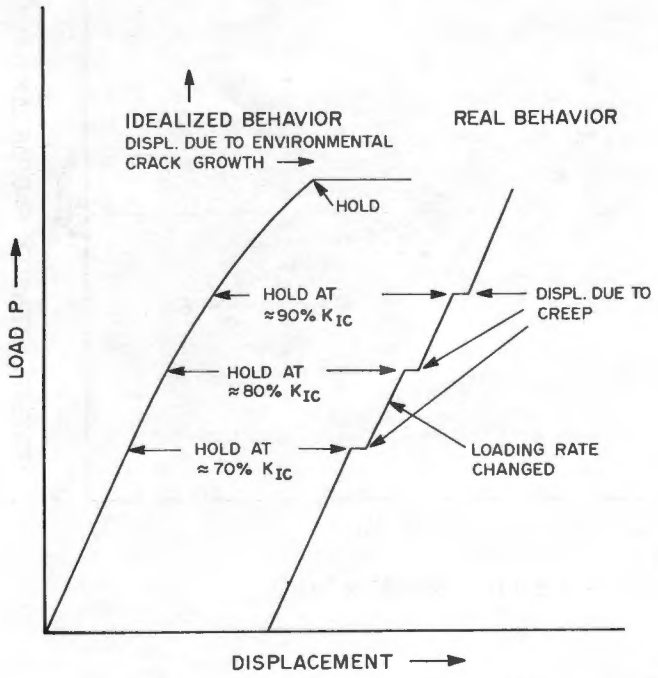

Figure 11. Schematic Diagram of Step Loading in Rising-Load Test for Al 7075-T6.

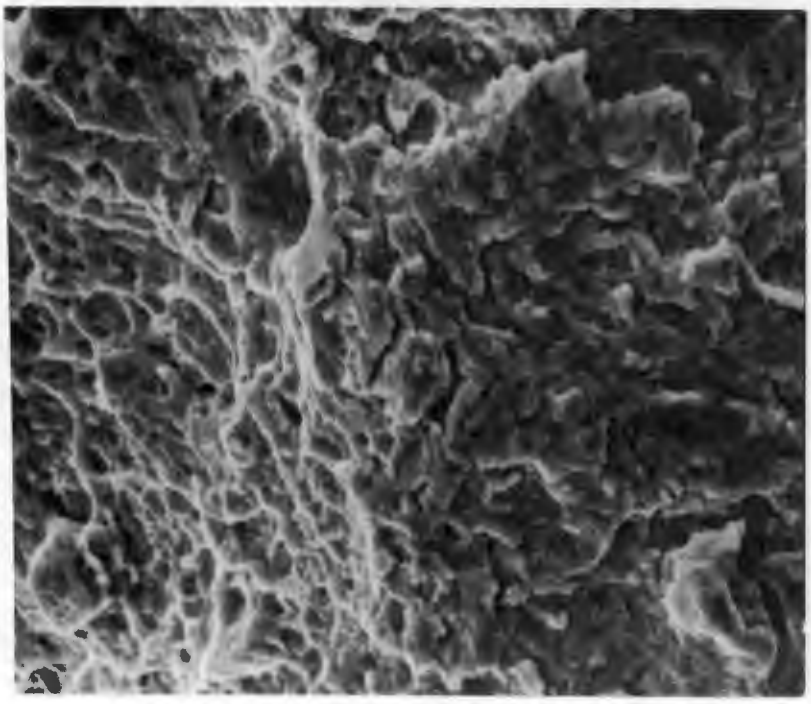

Figure 12(b). Fracture Surface of 1240 MPa Steel Tested in 1000 ppm SO_2 + 80% RH Environment at 57.5 MPa $\sqrt{m}$ (×3500).

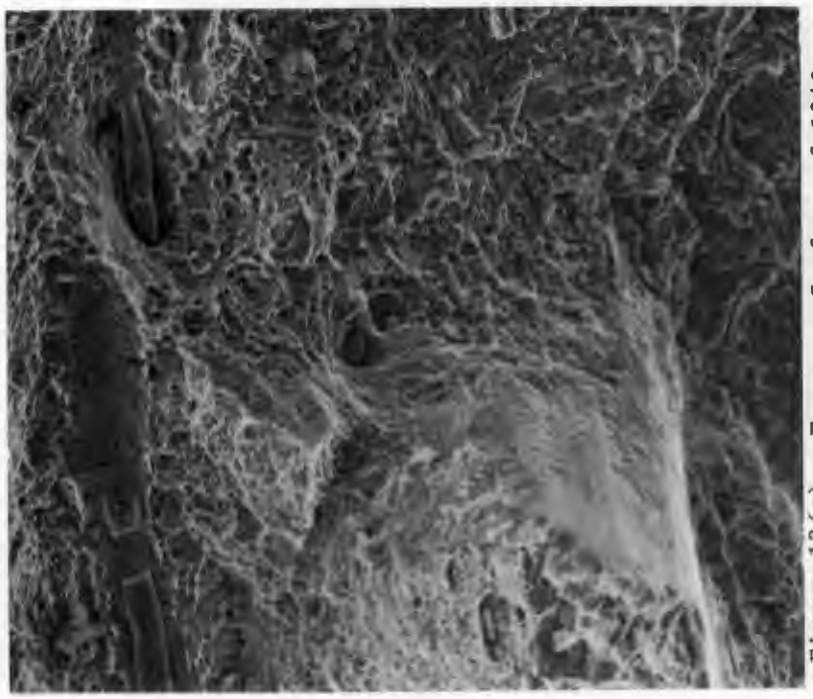

Figure 12(a). Fracture Surface of 1240 MPa Steel Tested in 1000 ppm SO_2 + 80% RH Environment at 57.5 MPa $\sqrt{m}$ (×600).

Figure 13(a). Ductile Morphology Obtained for 1440 MPa Steel, Resulting from Test in 1000 ppm SO_2 + 80% RH Environment in the Range 35-36 MPa $\sqrt{m}$ (×600).

Figure 13(b). Mixed-Mode Fracture Obtained for 1440 MPa Steel, Resulting from Testing in 1000 ppm SO_2 + 80% RH Environment at 40 MPa $\sqrt{m}$ (×1100).

Figure 13(c). Intergranular and Brittle Failure Obtained for 1440 MPa Steel Resulting from Test in 1000 ppm SO_2 + 80% RH Environment in the Range 45-46 MPa $\sqrt{m}$ (×1100).

Figure 14(a). Ductile Morphology Resulting from Test Conducted in Dry Nitrogen (×2200).

Figure 14(b). Higher Magnification of 14(a) Showing Dimple Rupture (×5000).